第 24 卷第 5 期 无 机 化 学 学 报 Vol.24 No.5
2008 年 5 月 CHINESE JOURNAL OF INORGANIC CHEMISTRY 715~722

一种通过纳米粒子的组装制备基于二氧化铈中孔材料的简易方法

乐 琳* 张晓鸣
(食品科学国家重点实验室,食品学院,江南大学,无锡 214122)

摘要: 用 HF 或者 HCl 作联合剂,三嵌段共聚物表面活性剂作模板剂,通过二氧化铈纳米粒子(或者过渡金属掺杂的二氧化铈纳米粒子)组装形成具有热稳定和晶化孔壁的基于二氧化铈的中孔材料。焙烧该合成的超分子模板中孔结构的材料可以形成具有高比表面的基于二氧化铈的中孔材料,这些中孔材料用不同的光谱技术表征。通过 D_2-OH 交换测得的二氧化铈表面的羟基在组装过程和中孔材料的稳定性方面至关重要。联结剂中的卤素离子(F 和 Cl 离子)可以替代中孔材料的表面羟基,从而影响这些中孔材料的结构稳定性和光学活性, 而用具有 3 d 的过渡金属在组装前掺杂二氧化铈纳米粒子可以显著地提高中孔材料的光学活性,这种提高主要归结为通过掺杂可以促使能量转移的提高。

关键词: 二氧化铈; 组装; 中孔结构; 催化
中图分类号: O614.33+2 **文献标识码**: A **文章编号**: 1001-4861(2008)05-0715-08

A Facile Approach to Mesoporous Ceria-based Materials by Assembly of Nanoparticles

YUE Lin* ZHANG Xiao-Ming
(*State Key Laboratory of Food Science and Technology, School of Food Science and Technology, Jiangnan University, Wuxi, Jiangsu* 214122)

Abstract: A facile approach to thermally stable and crystalline mesoporous ceria-based materials has been developed via assembly of ceria or transition metal doped ceria nanoparticles with HF or HCl as the binding agent and a triblock copolymer surfactant as the template. High surface area mesoporous ceria-based materials were obtained by calcination of the supramolecular-templated mesostructures and were characterized by using various spectroscopic techniques. The surface OH groups of ceria, quantitatively measured by D_2-OH exchange, are important both for the assembly process and for the stability of the mesoporous ceria. The halogen ions in the binding agents, fluorides or chlorides, can substitute the surface OH groups and affect the structural stability and the optical activities of the mesoporous ceria. The optical activity of the ceria nanoparticles was significantly improved by doping with 3 d transition metals before the assembly mainly due to the enhancement of energy transfer by the doping.

Key words: ceria; assembly; mesostructure; catalysis

Mesoporous materials derived from metal oxides instead of silicate frameworks are very useful in many aspects, such as catalysis, adsorption, sensors and nano devices[1~2]. A series of metal oxides with such structures have been synthesized via various pathways with condensation of metal oxo ions from soluble precursors[3~7]. Their poor thermal stability compared with the mesoporous silicate materials, however, limits their applications[8~11]. In 2001, Ying et al[12] reported a supramolecular templating approach for the preparation of crystalline mesoporous metal oxides with a triblock copolymer as the template. They obtained a thermal stable

收稿日期:2007-09-18。收修改稿日期:2008-01-26。
*通讯联系人。E-mail:yuelin@jiangnan.edu.cn; Tel:0510-85329059
第一作者:乐 琳,男,34 岁,博士研究生, 副教授;研究方向:食品化学。

mesoporous zirconia using inorganic colloidal zirconia nanoparticles instead of soluble zirconium precursors and the tungstate ions adsorbed on the surface of nano zirconia nanoparticles was used to bind the colloidal particles with the template polymers. The method has shown to be promising in enhancing the thermal stability of mesoporous metal oxides, where nanoparticles or crystalline nanoparticles stacked to bulk mesostructures[13~16]. Rolison[17] reviewed the importance of thus stacked nano-architectures used as catalysts.

Cerium oxide has attracted considerable interests for its technical importance[18~22]. Its unique support effect on loaded catalytic metals has been reported recently[23]. The mesoporous CeO_2 has been prepared via conventional method with soluble precursors[24,25], but it collapses at mild temperatures. Corma et al [15,16] and Niederberger groups[26] reported the synthesis of the ordered mesoporous CeO_2 with improved method using assembly of ceria nanoparticles. Both of their synthetic routes demonstrate the evaporation-induced self-assembly of pure sols of CeO_2, involving a careful and time-consuming pretreatment to purify and concentrate the nanoparticle dispersions.

The band gap of CeO_2 was reported as 3.2 eV[27], attributed to an $O2p \rightarrow Ce4f$ transition. CeO_2, however, is generally not considered as photoactive material. Esch et al[28] in their recent work on the electron localization of CeO_2 with the help of high-resolution scanning tunneling microscopy revealed that the defects of CeO_2 were difficult to move, and they concluded that the Ce^{3+}, or the electron trapped at 4*f* level, could not move at ambient temperatures. The results revealed the reason, at least one of the reasons, for inactive photo properties of CeO_2. The exciton(Ce^{3+}-O^-), if included in photo absorption of ceria, should be difficult to move or diffuse to surface at ambient temperatures and contribute little to the surface reactions. Doping the CeO_2 with 3*d* transition metal ions in bulk may be a promising method to improve the photo activity or ceria by enhancing the energy transfer,thus beneficial for the reactions at the surface of the ceria-based mesoporous materials.

In this report, a facile route is suggested for synthesis of the mesoporous ceria-based materials with ~5 nm CeO_2 or transition metal doped CeO_2 nanoparticles as building blocks and a triblock copolymer as the template. Inorganic acid HF or HCl is used as the binding agent for the assembly. The normal or doped CeO_2 nanoparticles were prepared via a simple solution process and were used for assembly without any further purifications or pretreatments. This method can be used for mass production of thermally stable mesoporous ceria-based materials with high surface areas. Our results on photocatalytic degradation of methylene blue (MB) show that doping the ceria nanoparticles with 3*d* transition metals significantly improves the photocatalytic activity of the mesoporous ceria-based materials. The measurement of the surface OH groups with D_2-OH exchange indicates that the density of OH groups affects the structural stability and the photocatalytic activities.

1 Experimental

All chemicals were purchased and used without further purification. $FeCl_3 \cdot H_2O$、$MnSO_4 \cdot H_2O$、$CoCl_2 \cdot 6H_2O$、$Ti(SO_4)_2$、$Ce(NO_3)_3$ and $NH_3 \cdot H_2O$ were purchased from Shanghai Chemical Reagents Company.

CeO_2 nanoparticles (~5 nm, denoted as Ce-NP) were prepared via a simple solution process. 10 mL $NH_3 \cdot H_2O$ solution (25wt%) was mixed with 200 mL deionized water under vigorously stirring and with oxygen gas bubbled into the solution through a gas distributor. 70 mL aqueous solution of 30 mmol $Ce(NO_3)_3$ was pumped continuously into the above vigorous stirred ammonia solution. The purple precipitate gradually turned to pale yellow with the oxidation of Ce(Ⅲ) to Ce(Ⅳ). The resulting slurry was stirred overnight at 293 K. The yellow precipitate was then washed by water and recovered by centrifugation. In order to clarify the effect of dopant on energy transfer of the ceria nanoparticles, The molar rate of Ce^{3+} to dopant 3*d* transition metal ions (Fe^{3+}, Mn^{2+}, Co^{2+} and Ti^{4+}) was 100∶5. Salt of dopant was respectively dissolved in aqueous solution of $Ce(NO_3)_3$.

The assembly of ceria or doped-ceria nanoparticles was performed with two procedures:

(a) 10 mL of a 0.6 mol·L^{-1} CeO_2 or doped CeO_2

colloidal suspension at pH value of 2 adjusted with 2 mol·L^{-1} hydrochloric acid was added to 8 mL aqueous solution of 0.72 g P123(Pluronic P123 surfactant, MW-5800, BASF). The mixture was stirred at 293 K for 24 h and followed by aging at 318 K for 48 h without stirring. The precipitate was collected by centrifugation and dried at room temperature and then calcined at 573 K for 6 h in air, denoted as Ce-HCl.

(b) 10 mL of a 0.6 mol·L^{-1} CeO_2 or doped CeO_2 colloidal suspension at pH value of 3 adjusted by hydrofloric acid was added to 8 mL aqueous solution of 0.72 g P123. The resulted homogeneous dispersion was stirred for 24 h at room temperature and allowed to evaporate in a film evaporator. The as-synthesized sample was calcined at 573 K for 6 h in air, denoted as Ce-HF.

The XRD patterns of the products were recorded using a Phillip X′ pert pro Advance Powder X-ray diffractometer with Cu $K\alpha$ irradiation (λ=0.154 06 nm) and a graphite monochromator. The X-ray source was operated at 40 kV and 40 mA. HRTEM micrographs were obtained with a FEI Tecnai G^2 20S-TWIN electron microscopy operating at an acceleration voltage of 200 kV. Samples for TEM measurements were suspended in ethanol and ultrasonically dispersed. Drops of the suspensions were applied to a carbon-coated copper grid. FTIR data was collected on a Bruker Vector22 spectrometer. The samples were mixed with KBr and pressed into pellets. Nitrogen adsorption/desorption isotherms were recorded using a micromeritics ASAP 2020 equipment. Before N_2 adsorption, the sample was outgassed under vacuum at 573 K for 3 h. The pore size distribution curves were obtained from the desorption branch calculated by the Barrett-Joyner-Halenda(BJH) method. TG analyses were performed in dry flowing air (5 mL·min^{-1}) on a STA449C-Thermal Star 300 at a heating rate of 10 K·min^{-1}. The ultraviolet-visible(UV-Vis) diffuse reflectance spectra were recorded at room temperature using a JASCO V-550 spectrophotometer (Japan) equipped with an integrating sphere with $BaSO_4$ as reference. The density of surface OH groups was measured by D_2-OH exchange technique. The HD evolution was monitored by mass spectrometer (Inficon Transpector 2) at mass to charge ratio of 3. Ar was used as internal standard for calculation. Samples were heated in 100 cm^3·min^{-1} of 20% O_2/He at 523K for 1 h and cooled down to room temperature in dry helium. Then the carrier gas was switched to 5% D_2/Ar, and the samples were heated at 5 K·min^{-1} to perform D_2/OH exchange.

The optical-catalytic degradation of aqueous methylene blue(MB) was conducted in a NDC photo-reactor equipped with a 500 mL cylindrical Pyrex vessel irradiated directly by a high pressure mercury lamp(250 W). The emission lines of the lamp are 365 nm(in 100% strength), 313 nm(20%), 254 nm(20%) and 410 nm (2%). In a typical run, 0.15 g of the catalyst was suspended in 500 mL MB solution in the dark for 100 min to reach the adsorption equilibrium prior to the reaction. During the optical-reaction, samples were collected at selected time intervals for analysis. The catalyst powders were removed by centrifugation and the residual concentration of MB was determined spectra-photometrically. The rate constants of the reaction are obtained by fitting the MB concentration using the first order kinetic equation on the basis of catalyst weight.

2　Results and discussion

The structural characterization of the samples is presented in the following paragraphs with mesostructured ceria as the representative. All the samples synthesized with HF or HCl as binding agent exhibit a low-angle diffraction maximum in their low angle X-ray diffraction (LAXD) patterns before and after the removal of the template, as shown in Fig.1. The sample Ce-HCl with ceria nanoparticles as building blocks and HCl as binding agent gives its (100) diffraction peaks at 2θ= 1.12° and 1.28°, respectively for the as-synthesized and calcined samples. For the sample Ce-HF, corresponding diffraction peaks are observed at 2θ=0.78° and 0.84°. These suggest a mesostructure for all the samples. The shift to higher angle of the diffraction peak by calcination reveals slight contraction of the mesostructured ceria upon surfactant removal. Extended XRD patterns indicate crystalline CeO_2 of the samples (insets of Fig.1).

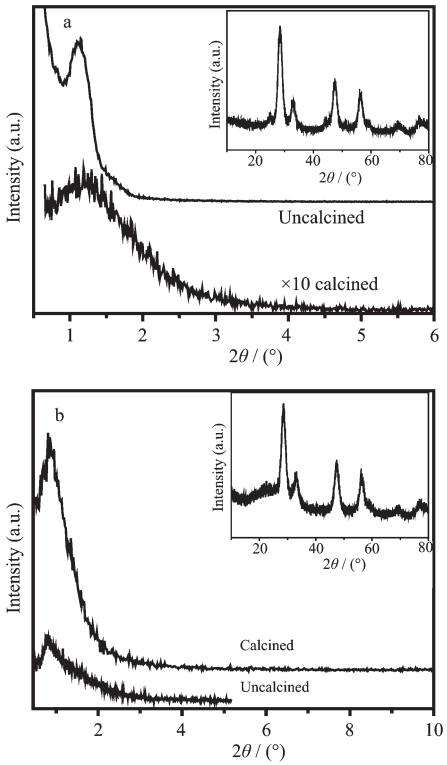

Fig.1 Low angle XRD patterns of mesoporous CeO_2 prepared with (a) HCl and (b) HF as binding agent. Calcination temperature was 573 K

The mesoporous ceria are found to possess high porous structures, as shown by TEM observations (Fig.2). The ceria nanoparticles included in the bulky mesostructured ceria are crystalline and in size of ~5 nm, revealed by HRTEM photos (inset of Fig.2). The pores appear to be interconnected and in worm like morphology. The porous structure seems to be not so ordered in a large area but aligns well in a small region, because the ceria nanoparticles are directly used as building blocks for large scale. The type IV nitrogen sorption isotherms show that the obtained ceria are typically mesoporous materials (Fig.3). Their specific BET surface area are ca. 133 $m^2 \cdot g^{-1}$ for Ce-HCl and 126 $m^2 \cdot g^{-1}$ for Ce-HF after calcination at 573 K for 6 h. Very narrow peaks appear in the distribution curves of pore diameter, respectively centered at 3.6 nm (Fig.3a, Ce-HCl) and 4.0 nm(Fig.3b, Ce-HF). The pore sizes calculated from N_2 adsorption are in fair agreement with the TEM results (~4.5 nm). With the lattice dimension given by XRD ($a_0=2d_{100}/\sqrt{3}$) and the pore diameter, the wall thickness can be calculated to be ~4.4 nm for Ce-HCl and ~8.0 nm for Ce-HF, respectively, much thicker than that of typical siliceous MCM41 (~1.0 nm). Comparing the current mesoporous ceria with the M41s silica, the greater molecular weight and much thicker walls of the pores should be responsible for the relative lower BET specific surface areas possessed by the meso-ceria.

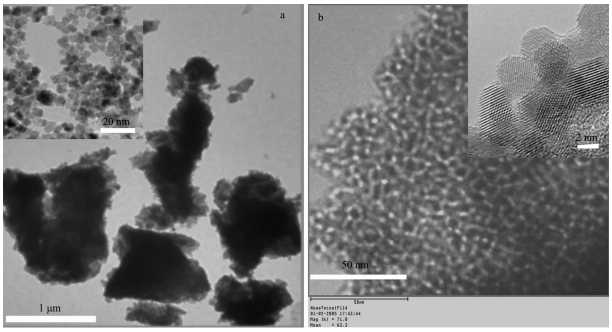

Fig.2 TEM images. (a) Typical morphology of the mesostructured ceria-based materials. Inset is the typical morphology of the nanoparticles. (b) Enlarged mesoporous structure of the ceria

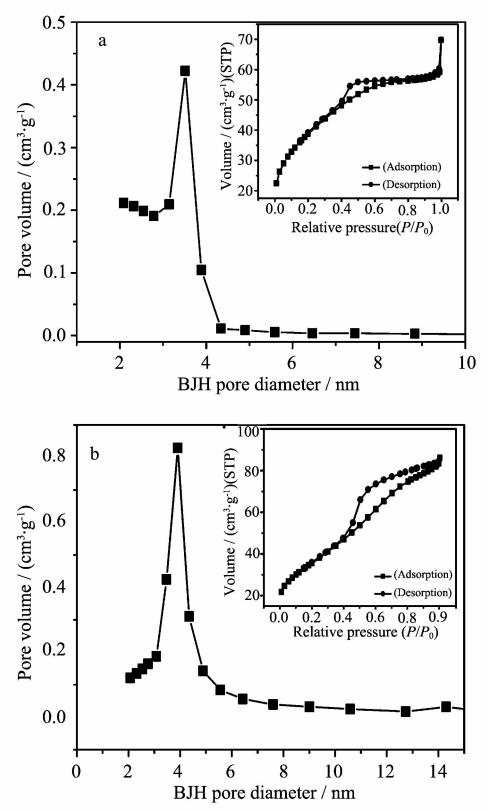

(a) HCl; (b) HF were used as binding agent

Fig.3 Nitrogen adsorption-desorption isotherms and pore size distribution of the calcined mesostructure ceria

Table 1 lists the data about the texture properties of the samples before and after the heat treatment at

Table 1　Texture properties of the samples treated at various temperatures

Sample	Temp. / K	D^{*1} / nm	Surface area / ($m^2 \cdot g^{-1}$)	Pore size*2 / nm	Pore volume / ($cm^3 \cdot g^{-1}$)
Ce-HCl	573	5.6	133	3.6	0.108
Ce-HCl	773	9.2	65	3.8	0.091
Ce-HCl	973	16.2	24	3.8	0.034
Ce-HF	573	5.7	126	4.2	0.154
Ce-HF	773	8.5	87	6.3	0.235
Ce-HF	973	12.7	51	6.6	0.202
Ce-HF-HT*3	773	8.7	85	6.8	0.112
Ce-HF-HT*3	973	13.3	44	7.6	0.103

*1 Ceria crystal size calculated from XRD data using Scherrer equation(Average value for 111 and 220 planes)

*2 Measured by N_2 adsorption. *3 100% steam treatment

various temperatures. It can be seen that the obtained mesoporous ceria is much stable, especially for the sample Ce-HF with HF as binding agent. The specific surface area of the Ce-HF is still very large (44 $m^2 \cdot g^{-1}$) after the treatment at 973 K in 100% steam, considering that the molecular weight of CeO_2 is 3 times of silica. Fig.4 shows the FTIR spectra of the samples. Some peaks attributed to surface adsorbed CO_3^{2-}(1 520 cm^{-1}) and NO_3^-(849, 1 057, 1 345 cm^{-1}) species are observed for the ceria nanoparticles prepared with $Ce(NO_3)_3$ as precursor and $NH_3 \cdot H_2O$ as reactant in air. These adsorbed species were removed during assembly for mesostructured ceria, due to the addition of HCl or HF. The IR spectra of the as-synthesized mesoporous CeO_2 indicate the presence of organic templates with the typical absorption at 2 920, 2 850 and 1 480 cm^{-1} from the aliphatic C-H vibrations. For the template removed samples, the corresponding band intensities are drastically reduced, indicating the efficient removal of the organic molecules. Fig.5 depicts the thermal analysis results, two distinct weight losses are observed, respectively arising from the desorption of water (below 200 ℃) and the decomposition of the organic template (250~290 ℃). The total amount of the organic template presented in the sample is 25wt% for Ce-HCl and 35wt% for Ce-HF, reflecting stronger interaction between F^- functionalized surface of ceria and protonized surfactant P123. This may be the reason of better stability of Ce-HF compared to Ce-HCl. The very narrow temperature window for combustion of organic template implies the ordered structure of the materials. In addition, the easy removal of the surfactant from the mesostructured ceria is partially due to the good catalytic oxidation property of ceria[29], larger pore sizes and the easy oxidation property of P123 (one carbon combines with one oxygen in its molecule). The calcination at 573 K in air can entirely remove organic surfactant from the mesostructured ceria.

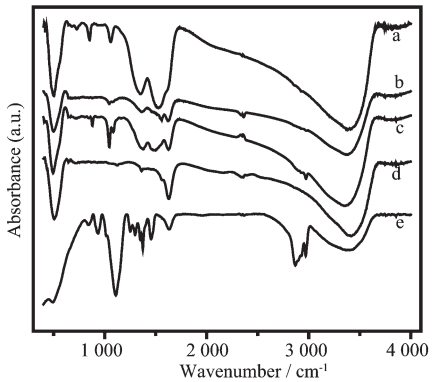

Fig.4　FTIR spectra. (a) as-synthesized ceria nanoparticles (Ce-NP); (b) calcined Ce-HCl; (c) uncalcined Ce-HCl; (d) calcined Ce-HF, (e) uncalcined Ce-HF

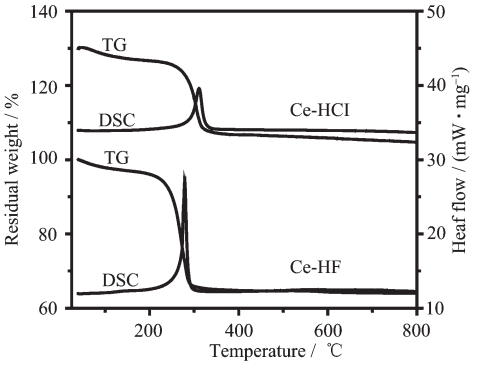

Fig.5　TG and DSC curves for the as-synthesized mesostructured CeO_2

As discussed for synthesis of SBA-15[30], the current assembly of ceria nanoparticles occurs through ($S^{\circ}H^{+}$)($I^{-}C^{+}$) charge interactions, i.e., Cl^{-} or F^{-} as I^{-}, positively charged ceria nanoparticles as C^{+} and the proton-bonded polymer surfactants as $S^{\circ}H^{+}$. At the pH values in this work, the above mode should be prevailing. The ceria nanoparticles are positively charged, since the point-of-zero charge of CeO_2 is about 8.1[31], and the structure of protonized P123 has been well established in literature[32]. It is critical for the formation of the mesostructured ceria that the above two components are tied together by the HCl or HF at 318 K for some time without stirring.

Some 3*d* transition metals were doped to the ceria nanoparticles via co-precipitation method, and TEM observation (not shown) indicated that the doped ceria nanoparticles had similar morphology to the pure ceria. The doped ceria nanoparticles can also be assembled to mesostructures via similar synthetic strategy as pure mesostructured ceria. Fig.6 depicts their UV-Vis spectra. The absorption bands for charge transfer(O2*p*-Ce4*f*) for the doped ceria samples extend to longer wavelength compared to pure meso ceria, indicating that the 3*d* transition metals supply lower unoccupied orbitals than Ce4*f*, the transition from O2*p* to the unoccupied orbitals

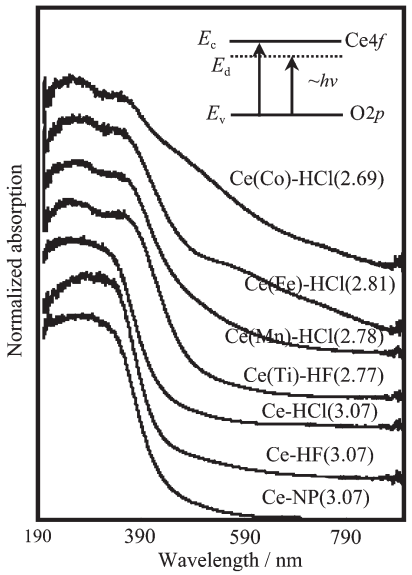

Fig.6 UV-Vis spectra of some mesoporous CeO_2 doped with 3*d* transition metals.The figures in parentheses were the energy for charge transition(eV)

needs lower energy, the doped samples are more efficient for absorption of visible light. For the current assembly methodology, it is important that the surface of the ceria nanoparticles is functionalized by F^{-} or Cl^{-} ions, which is possible to substitute the surface hydroxyl groups and then to influence the property of the materials to some extent when they are used as catalysts or catalyst supports. The residue fluoride or chloride on the surface of the mesoporous ceria is indeed detected by XPS. Table 2 lists the change of surface composition of the mesoporous ceria with calcination temperature. A lot of fluorides or chlorides are detected on as-synthesized samples, but they can be totally removed by calcination at high temperature in air.

Table 2 Surface composition of the samples determined by XPS

Sample	Calcination temperature / K	Surface atomic ratio
Ce-HF	573 6 h)	Ce:O:F=1:1.61:0.49
Ce-HF	773(6 h)	Ce:O:F=1:2.0:0.0
Ce-HCl	uncalcined	Ce:O:Cl=1:1.86:0.11
Ce-HCl	573(3 h)	Ce:O:Cl=1:1.93:0.06
Ce-HCl	573(12 h)	Ce:O:Cl=1:1.94:0.0
Ce-HCl	773(6 h)	Ce:O:Cl=1:1.95:0.0

The adsorption of halogen ions on the surface of the mesoporous ceria is also proved by D_2-OH exchange measurement. The density of surface hydroxyls of the samples is detected by technique of D_2-OH exchange[33~34]. Fig.7 shows the HD evolution curves during the D_2-OH exchange. For ceria nanoparticles calcined at 573, 673 or 773 K, the maximum rates of HD evolution are observed at the same temperature(523 K). The hydroxyl density decreases with the increase of calcination temperature. While for Ce-HCl, the HD evolution peak centers at ~643 K, about 120 K higher than that of ceria nanoparticles, indicating the different surface property of Ce-HCl compared to ceria nanoparticles. It appears that the surface chlorides have effects on the D_2 dissociation, which is the rate-determining step in D_2-OH exchange. Compared to ceria nanoparticales, only 35% hydroxyls are reserved after the assembly(Ce-HCl). Noteworthy that totally no hydroxyls are detected for Ce-HF, indicative of the replacement of the surface hydroxyls of ceria by fluorides.

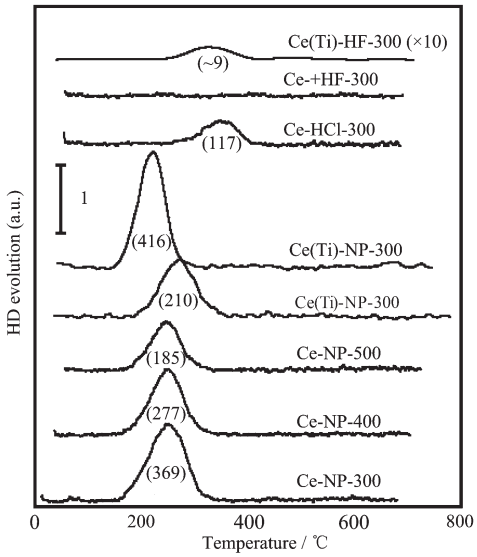

Fig.7　HD evolution curves during D_2-OH exchange. The figures in parentheses were the OH density of the samples($\mu mol \cdot g^{-1}$)

The photocatalytic degradation of methylene blue (MB, $C_{16}H_{18}ClN_3S \cdot 3H_2O$) is tested on the mesoporous ceria-based materials to check the dope effects. The rate constants of the reaction, obtained by fitting the reaction data using the first order kinetic equation, are shown in Fig.8. The doping of transition metal significantly enhances the photo activity for MB reaction. The most active sample is Ce (Co)-HCl, while the mesoporous samples prepared with HF method give lower

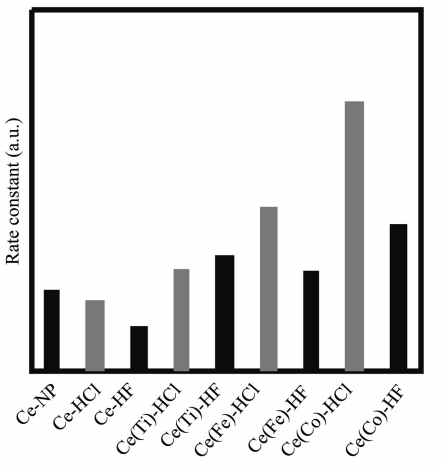

Fig.8　Catalytic property of the samples (calcined at 573 K for 6 h) on photocatalytic degradation of methylene blue(MB) at room temperature. The rate constants were calculated from the fitting of reaction data, i.e. the variation of MB concentration with reaction time under photo irradiation

activity, implying fluorated surface is detrimental to the photocatalysis. Generally, for the current mesoporous ceria-based samples, high density of surface OH groups is good for their photocatalytic activity. The calcination of the mesoporous ceria-based samples at higher temperatures, on which OH density decreases, results in much depressed photocatalytic activity (not shown). Only the changes in hydroxyls, however, are not enough to account for the changes in the photocatalytic activity. Hence, we think both the electrons, resulting in oxygen radicals, and the holes, leading to hydroxyl radicals, are involved in the reaction. Moreover, the former is more important[35~38]. Because the surface area of all the samples are approximately the same and the energy of the Hg light used for the optical reaction is focused at the wavelengths shorter than 400 nm (365 nm 100%, 313 nm 20%, 254 nm 20%, 410 nm 2%), it may be reasonable to attribute the improved photocatalytic activity of the doped ceria to the enhancement of energy transfer from the doping. Further works in this respect are in progress.

3　Conclusion

In conclusion, thermally stable and crystalline mesoporous ceria-based materials can be obtained by a facile but efficient approach with ceria or doped ceria nanoparticles as building blocks and HF or HCl as binding agent. The formation of the mesostructures may be attributed to the charge interaction among the nanoparticles, P123 micelles and halogen anions. Calcination of the supramolecular-templated mesostructures yields the mesoporous ceria-based materials with high surface areas, of which surface density of OH groups is affected by the assemble process. The binding agents change the density of OH groups of the meso-ceria, which increases their structural stability but detrimental to their optical activities. Doping the ceria nanoparticles with transition metals significantly improves their optical activity, which may be due to the enhancement of energy transfer.

References:

[1] Corma A. *Chem. Rev.*, **1997**,**97**:2373~2420

[2] Mamak M, Coombs N, Ozin G A. *Adv. Funct. Mater.*, **2001**, **1**:59~63

[3] Antonelli D M, Ying J Y, Angew. *Chem. Int. Ed. Engl.*, **1995**, **34**:2014~2017

[4] Antonelli D M, Ying J Y, Angew. *Chem. Int. Ed. Engl.*, **1996**, **35**:426~430

[5] Yang P D, Zhao D Y, Stucky G D, et al. *Nature*, **1998**,**396**: 152~155

[6] Kang M, Yi S H, Lee H I, et al. *Chem. Commun.*, **2002**,1944 ~1945

[7] Dong A G, Ren N, Tang Y, et al. *J. Am. Chem. Soc.*, **2003**, **125**:4976~4977

[8] Stein A, Fendorf M, Mallouk T E, et al. *Chem. Mater.*, **1995**,**7**: 304~313

[9] Ciesla U, Schacht S, Stucky G D, et al. *Angew. Chem. Int. Ed. Engl.*, **1996**,**35**:541~543

[10]Elder S H, Gao Y, X Li, et al. *Chem. Mater.*, **1998**,**10**: 3140~3145

[11]Yang P D, Zhao D Y, Stucky G D, et al. *Chem. Mater.*, **1999**, **11**:2813~2826

[12]Wong M S, Jeng E S, Ying J Y. *Nano letters*, **2001**,**1**:637~642

[13]Rana R K, Zhang L Z, Gedanken A, et al. *Langmuir*, **2003**, **19**:5904~5911

[14]Zhou Y, Antonietti M. *J. Am. Chem. Soc.*, **2003**,**125**:14960~ 14961

[15]Corma A, Atienzar P, Garcia H, et al. *Nature Materials*, **2004**,**3**:394~397

[16]Ching J Y C, Cobo F, Corma A, et al. *Chem. Eur. J.*, **2005**,**11**: 979~987

[17]Rolison D R. *Science*, **2003**,**299**:1698~1701

[18]Trovarelli A. *Catal. Rev. Sci. Eng.*, **1996**,**38**:439~520

[19]Flytzani-Stephanopoulos. *MRS Bull.*, **2001**,**26**:885~889

[20]Corma A, López-Nieto J M. *Handbook on the Physics and Chemistry of Rare Earths*, Amsterdam : Elsevier, **2000**.269

[21]Steele B C H. *Solid State Ionics*, **2000**,**129**:95~110

[22]Murray E P, Tsai T, Barnett S A. *Nature*, **1999**,**400**:649~ 651

[23]Guzman J, Carrettin S, Fierro-Gonzalez J C, et al. *Angew. Chem. Inter. Ed.*, **2005**,**44**:4778~4881

[24]Terribile D, Trovarelli A, Llorca J, et al. *J. Catal.*, **1998**,**178**: 299~308

[25]Lyons D M, Ryan K M, Morris M. *J. Mater. Chem.*, **2002**,**12**: 1207~1212

[26]Deshpande S, Pinna N, Niederberger M, et al. *Small*, **2005**, **1**:313~316

[27]Orel Z C, Orel B. *Phys. Status Solidi B.*, **1994**,**186**:33~36

[28]Esch F, Fabris S, Zhou L, et al. *Science*, **2005**,**309**:752 ~755

[29]Zhou K B, Wang X, Sun X M, et al. *J. Cata.*, **2005**,**229**:206 ~212

[30]Zhao D Y, Feng J L, Stucky G D, et al. *Science*, **1998**,**279**: 548~552

[31]Ardizzone S, Trasatti S. *Advances in Colloid and Interface Science*, **1996**,**64**:173~251

[32]Bailey Jr F E, Callard R W. *J. Appl. Polym. Sci.*, **1959**,**1**:56 ~62

[33]Martin D, Duprez D. *J. Phys. Chem. B.*, **1997**,**101**:4428~4436

[34]Thomas C, Vivier L, Travert A, et al. *J. Catal.*, **1998**,**179**:495 ~502

[35]Hoffmann M R, Martin S T, Choi W, et al. *Chem. Rev.*, **1995**, **95**:69~96

[36]Gerischer H, Heller A. *J. Electrochem. Soc.*, **1992**,**139**:113 ~118

[37]Wang C M, Heller A, Gerischer H. *J. Am. Chem. Soc.*, **1992**, **114**:5230~5234

[38]Gerischer H, Heller A. *J. Phys. Chem.*, **1991**,**95**:5261~5267